Interaction between confined phonons and photons in periodic silicon resonators

A. Iskandar,[1,2] A. Gwiazda,[2] J. Younes,[1] M. Kazan,[1,*] A. Bruyant,[2] M. Tabbal,[1] and G. Lerondel[2]
[1]*Department of Physics, American University of Beirut, P.O. Box 11-0236, Riad El-Solh, Beirut 1107-2020, Lebanon*
[2]*Laboratoire de Nanotechnologie et d'Instrumentation Optique, ICD, CNRS UMR 6281, Université de Technologie de Troyes, 10010 Troyes, France*

(Received 1 October 2017; published 30 March 2018)

In this paper, we demonstrate that phonons and photons of different momenta can be confined and interact with each other within the same nanostructure. The interaction between confined phonons and confined photons in silicon resonator arrays is observed by means of Raman scattering. The Raman spectra from large arrays of dielectric silicon resonators exhibited Raman enhancement accompanied with a downshift and broadening. The analysis of the Raman intensity and line shape using finite-difference time-domain simulations and a spatial correlation model demonstrated an interaction between photons confined in the resonators and phonons confined in highly defective regions prompted by the structuring process. It was shown that the Raman enhancement is due to collective lattice resonance inducing field confinement in the resonators, while the spectra downshift and broadening are signatures of the relaxation of the phonon wave vector due to phonon confinement in defective regions located in the surface layer of the Si resonators. We found that as the resonators increase in height and their shape becomes cylindrical, the amplitude of their coherent oscillation increases and hence their ability to confine the incoming electric field increases.

DOI: 10.1103/PhysRevB.97.094308

I. INTRODUCTION

Due to the need for low-cost, clean, and sustainable energy sources to replace the shrinking supply of fossil fuels, considerable efforts have been made in pursuit of the highly efficient photovoltaic effect in silicon (Si), which is a material known for its ease of fabrication. Indeed, this is not an easy struggle because of the high reflectivity and indirect electronic band structure of Si. The high reflectance of the incoming radiations from the Si surface drastically reduces the number of photons that contribute to the photovoltaic generation of electricity, and the Si indirect electronic band structure disfavors the electron photoexcitation from the maximum of the valence band to the minimum of the conduction band. In fact, the electron excitation from the maximum of the valence band to the minimum of the conduction band in crystalline Si requires the assistance of phonons to make up for the momentum mismatch between the maximum of the valence band and the minimum of the conduction band. Therefore, the significant enhancement in the efficiency of the photovoltaic effect in Si requires reduction in lossy light processes and coupling between trapped photons and phonons confined in low-translational-symmetry structures where the total momentum needs not be conserved in order to excite electrons from the maximum of the valence band to the minimum of the conduction band [1].

The surface structuring has shown potential in reducing the reflectance and enhancing the interaction between light and matter. As such, there have been reports on significant reflectance reduction over a wide spectral range through surface structuring in the form of periodic or random arrays of micron-sized pyramids or rods [2–11]. On the other hand, Raman light scattering measurements have revealed evidence of phonon confinement in nanosized crystalline zones in highly defective crystals whereby the phonon selection rule is relaxed [12,13]. Thus, micron-sized structures are required to reduce the reflectance of incident photons whereas nanosized crystallites are needed to relax the requirement of total momentum conservation and enhance the probability of the electron transition from the maximum of the valence band to the minimum of the conduction band.

It is well known now that plasmonic nanoresonators forward scatter normally incident light towards the substrate on which they are attached [14]. Although this process enhances the coupling between light and matter, it is much too lossy to confine photons. However, when identical plasmonic nanoresonators are arranged into a two-dimensional lattice such that the lattice period is comparable to the wavelength of the normally incident light, the fields scattered by the individual nanoresonators combine together to give rise to a field in the plane of the nanoresonator lattice [15,16]. If that field is spectrally close to the resonance frequency of the individual plasmonic nanoresonators, doubly degenerate hybrid light-plasmon collective modes (known as plasmonic lattice resonance modes) occur, inducing highly coherent plasmonic oscillations at all the lattice points [17]. This makes all the nanoresonators oscillate in a coherent fashion. This coherent oscillation of the nanoresonators causes the field scattered by one nanoresonator to be absorbed by the others [16], and consequently the electric field is confined in the nanoresonators. Similar to localized plasmon resonances in plasmonic nanoresonators, localized Mie resonances in dielectric resonators induce forward scattering and coupling of normally incident light into the substrate beneath the resonators [18–20], and localized

*mk140@aub.edu.lb

Mie resonances at two-dimensional lattice points induce highly coherent oscillations in the dielectric resonators, which leads to strong field confinement in the dielectric resonators [21,22].

On the other hand, the structuring of the Si surface in the form of periodic micron-sized resonators over a large area triggers the development of nanosized crystallites embedded in regions with high structural defect densities in the surface layers of the resonators. In these short spatial correlation zones, the phonon selection rule may be broken due to phonon confinement [23,24]. The tips of tiny Si nanowires also present potential short spatial correlation zones for breaking the phonon selection rules [25,26].

It follows from the discussion above that dielectric resonators periodically arranged over a large area with periodicity comparable to the incident photons wavelengths could have the potential to simultaneously confine the incident photons and generate confined phonons in their surface layers. In other words, dielectric resonators at lattice points can ensure the interaction between long-living confined photons and nanosized crystallites in which the phonon selection rule is broken. In this contribution, we first demonstrate that Si resonators at lattice points with periodicity comparable to the normally incident light wavelength efficiently confine the incoming light, which can interact with phonons confined in short correlation length crystals prompted by the structuring process. Then, we demonstrate the shape and size of Si resonators that best confine the incoming electric field and ensure its interaction with nanosized crystallites for high-efficiency Si-based optical devices. Raman spectroscopy has demonstrated a high potential for the evaluation of the confinement of the electric field [19,22]. In addition, the analysis of Raman line shape can be carried out to yield quantitative determination of the spatial correlation length in the measured material [1,12,13,27–29]. Therefore, we use Raman spectroscopy to evaluate the confined electric field and measure the crystallites' sizes in the surface layers of the Si resonators.

II. EXPERIMENTS

Resonators in the form of pillars and truncated cones were fabricated in Si by reactive ion etching (RIE) using a ZnO hard mask by a special technique called MUZ [30]. While ZnO can be easily dissolved chemically, it is difficult to dry etch. To define the mask patterns, interferential lithography using a 355-nm laser source was used. A square lattice with circular patterns of a period of 600 nm was created by a double exposure of the sample, whereby the diameter of the features could be controlled by changing the exposure time. The array lattice parameter was chosen that was close to the wavelength of the laser line used in the Raman measurements to stimulate optical resonance effects. Thereafter, Si etching was conducted in a Plassys MU400 reactor using a SF_6/O_2 gas mixture. A selectivity of about 100 was demonstrated with Si using ZnO as a hard mask [30]. The height of the resonators could be controlled by varying the etching time.

Three sets of samples were obtained. The first set consists of two samples (samples $S_{S,1}$ and $S_{S,2}$) in which the resonators have almost the same height. However, the resonators of the first sample are conelike, whereas the resonators of the second sample are pillarlike. The second set consists of three samples (samples $S_{M,1}$, $S_{M,2}$, and $S_{M,3}$). The height of the resonators in this set is greater than that of the resonators in the first set. The samples in the second set, like in the first set, differ only in that the shapes of their resonators are different. The third set consists of three samples (samples $S_{L,1}$, $S_{L,2}$, and $S_{L,3}$). The resonators in this set are the highest, and again the only difference between the samples is the shape of their resonators. Thus, within the same set, the only difference between the samples is the ratio of the diameter at the top of the resonators to the diameter at the bottom of the resonators. With the present arrangement of the samples, we will be able to investigate the effect of the resonators' height and shape on the confinement of the electric field and its interaction with phonons confined in nanosized crystallites. In Fig. 1, we present scanning electron micrographs (SEMs) of four different arrays as an illustration of the diversity of the Si resonators investigated in this work. In Table I, we present a detailed structural description of all the samples investigated.

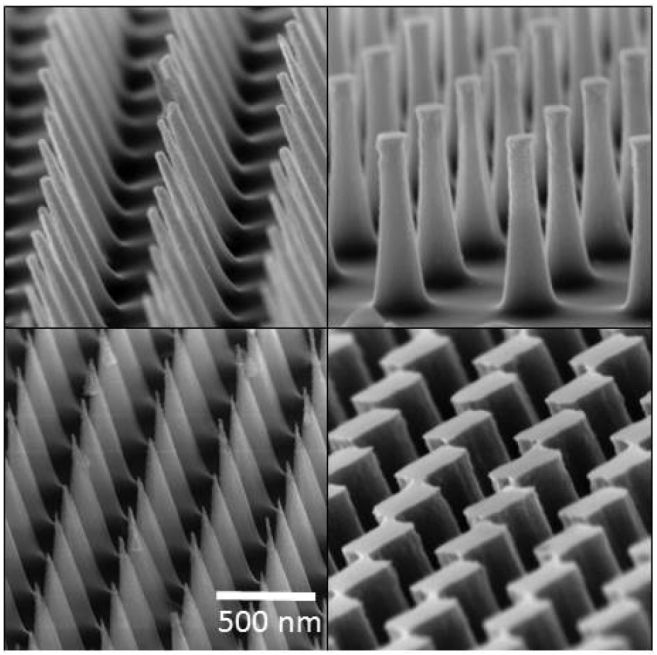

FIG. 1. Scanning electron micrographs (SEMs) of periodic arrays of Si resonators of different sizes and shapes.

Raman measurements were performed in the backscattering configuration using a 532-nm laser line from an Ar-ion laser. Very narrow slit widths, extremely low power, and long integration time were adopted to avoid spectrum distortion by sample heating and phenomena related to interaction of light with electrons. An 850-mm focal-length spectrometer with 1800 groves/mm holographic grating was used in the measurements.

III. RESULTS AND DISCUSSION

In infinite crystalline materials, the Raman shift and line shape are determined by the energy and lifetime of the optical phonon at the center of the Brillouin zone. Impurities and extended elastic fields (caused by internal or external stress), however, alter the energy and lifetime of the zone center

TABLE I. Detailed structural description of the samples and crystallites' size distributions in the surface layers of the Si resonators. The error on the crystallites' sizes and size distributions is estimated to not exceed 3%. The subscripts S, M, and L refer to short, medium, and long, respectively. An infinite spatial correlation length refers to an unconfined phonon (phonon in infinite crystal).

Set	Sample	Resonator height (nm)	Resonator bottom diameter (nm)	Resonator top diameter (nm)	Ratio of the top diameter to the bottom diameter	Average spatial correlation length (nm)	Size distribution skewness
I	$S_{S,1}$	450	134	15	0.112	∞	
	$S_{S,2}$	590	453	413	0.912	6.2	0.07
II	$S_{M,1}$	800	334	43	0.129	5	~0 (monodisperse)
	$S_{M,2}$	825	306	125	0.408	3.7	~0 (monodisperse)
	$S_{M,3}$	875	380	235	0.618	6.5	0.05
III	$S_{L,1}$	1150	450	100	0.222	6.5	0.2
	$S_{L,2}$	1280	650	190	0.292	4.3	~0 (Monodisperse)
	$S_{L,3}$	1240	291	159	0.546	4.1	~0 (Monodisperse)

optical phonon, and consequently modify the Raman shift and line shape [31–34]. In addition, the interaction between light and matter may trigger several mechanisms that can further distort the Raman spectrum. For instance, high laser powers can induce high concentrations of free carrier, and hence the induced free carriers' continuum gas can couple with the discrete phonon modes to give rise to the so-called Fano resonance [35], which usually results in an asymmetric Raman line shape [36,37]. Moreover, high laser powers can cause a local temperature rise, which reduces the lifetime of the excited phonons and weakens their energies. This temperature-related phenomenon further broadens the Raman peak and shifts it toward lower frequencies [38]. In nanosized crystallites, additional size effects combine with the effects described above, further distorting the Raman spectrum [39]. In fact, in nanosized crystallites, the Heisenberg uncertainty principle imposes the relaxation of the conservation of the total momentum, and consequently the relaxation of the requirement that only the zone center optical phonons participate in the Raman scattering processes. Thus, phonons away from the Brillouin zone center contribute to the response of the nanosized crystallite to an optical excitation. According to the Heisenberg uncertainty principle, all the phonons whose wave vectors are roughly equal to or smaller than the inverse of the crystallite size contribute to the response of the crystallite to an optical excitation [40–42]. This results in a further downshift and broadening of the Raman peak. It follows that the Raman shift and line shape may be determined by many effects combined together [43].

The samples investigated in this work consist of Si resonators periodically arranged in a two-dimensional lattice on a Si substrate, and the surface structuring of Si was made at low temperature to prevent any impurity diffusion. Hence, we do not expect any stress- or impurity-induced elastic fields contributing to the measured Raman spectra. In order to rule out the effect of laser heating and laser-induced Fano resonance, we have decreased the excitation laser power successively until both Raman peak position and broadening became independent of laser power. It is worth noting here that we found effects of Fano resonance and laser heating for a laser power as low as 0.2 $mW/\mu m^2$, which is five times lower than the reported threshold power for the effects of laser heating and Fano resonance [44,45] in Si nanocrystals. We address the reason behind this observation at the end of this section.

In order to be able to compare the Raman shift and line shape recorded from the structured samples with those recorded from a bare Si substrate, we multiplied the measured Raman spectra by constants to make them all of the same intensity. The obtained spectra will be referred to hereinafter as normalized Raman spectra. In Fig. 2, we illustrate normalized Raman spectra of some structured samples together with the Raman spectrum of a bare Si substrate. All the spectra are recorded by using a laser power of 0.1 $mW/\mu m^2$ and long integration time to avoid any effect of Fano resonance and laser heating. Compared to the Raman spectrum of the bare Si substrate, the spectra of the structured samples present a broadened and downshifted Raman peak. Since we have ruled out the effects of laser heating and Fano resonance, we confidently attribute this to phonon confinement. In other words, we attribute the

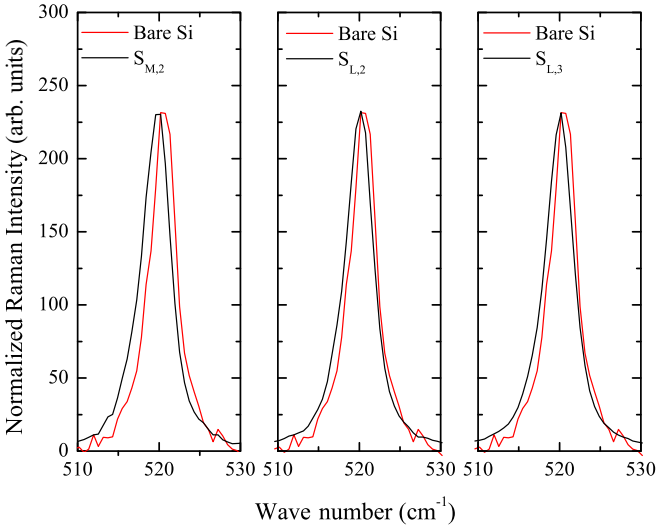

FIG. 2. Normalized Raman spectra of structured samples and a bare Si substrate. To guarantee a reasonable comparison between the Raman shift and line shape of structured samples and those of a bare Si substrate, the measured spectra were multiplied by constants to make them all of the same intensity.

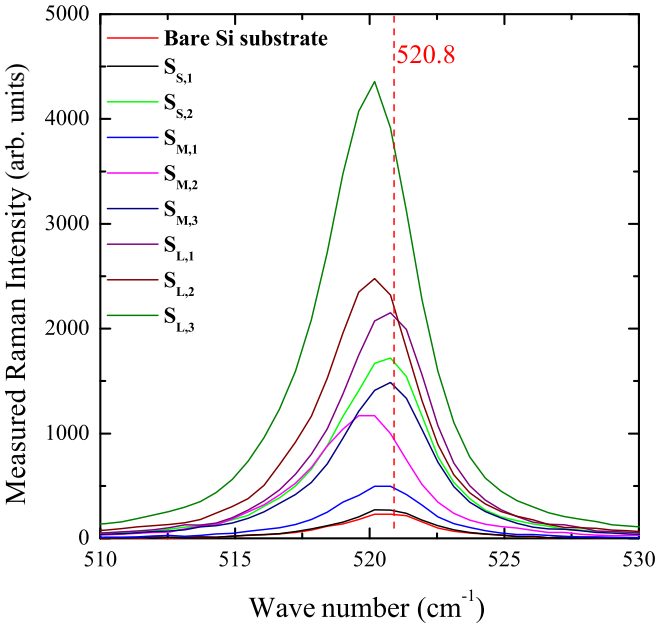

FIG. 3. As measured Raman spectra from the investigated structured Si substrates and a bare Si substrate. The position of the Raman peak of the bare Si substrate at 520.8 cm^{-1} is highlighted to illustrate the downshift of the Raman peaks corresponding to the structured Si substrates.

observed softening and broadening of the Raman resonance to nanosized crystallites embedded in highly defective Si in the surface layers of the resonators induced by the structuring process. This hypothesis is supported by previously reported Raman and thermal measurements demonstrating the presence of defect-induced confined phonons in large arrays of Si resonators [23,24,46].

In Fig. 3 we present the "as measured" Raman spectra. Besides the broadening and downshift of the Raman peak, Fig. 3 shows that the resonators induce a remarkable Raman enhancement. If the Raman spectra in Fig. 3 were corrected for the areal density of the resonators, the Raman enhancement would be of orders of magnitude. As mentioned above, the phonon confinement breaks the conservation of the total momentum and allows all the phonon modes whose wave vectors are equal to or smaller than $\frac{1}{D}$ (where D is the size of the crystallites in which the phonons are confined) to contribute to the sample's response to an optical excitation. This would indeed imply a Raman enhancement of the order of D^{-3} if we consider a phonon dispersion in a three-dimensional Brillouin zone. However, on the other hand, the Raman scattering efficiency is proportional to the interaction volume, which is roughly equal to D^3. Therefore, we believe that the observed Raman enhancement is not due to the phonon confinement effect. It is also known that isolated nanosized crystallites, or nanosized crystallites embedded in an amorphous medium with a very different index of refraction n, can show Raman enhancement due to electromagnetic resonances induced by local field effect and surface phonon modes [47–54]. However, since crystalline and amorphous Si have similar refraction indices, the Raman enhancement observed in our experiments cannot also be attributed to local field inducing electromagnetic resonances and surface modes contributing to the measured Raman spectra. Nonetheless, it has been demonstrated theoretically and experimentally that, similar to localized plasmon resonances in plasmonic nanoresonators, localized Mie resonances in dielectric resonators at the points of a two-dimensional lattice induce highly coherent oscillations in the dielectric resonators, which leads to strong field confinement in the dielectric resonators [21,22]. We believe that this is the only reasonable explanation of the Raman enhancement observed in our experiments. Therefore, we can conclude from the normalized Raman spectra illustrated in Fig. 2 and from the "as measured" Raman spectra illustrated in Fig. 3 that large arrays of Si resonators could ensure interaction between confined phonons and confined photons. In what follows, we shall examine the effect of the resonators' shape and size on the phonon and photon confinement.

A. Effect of the resonator shape in the first set of samples (resonator heights ranging between 450 and 590 nm)

The Raman spectra of the samples of the first set (samples $S_{S,1}$ and $S_{S,2}$) and finite-difference time-domain (FDTD) simulations of the electric field distribution on the surfaces of samples $S_{S,1}$ and $S_{S,2}$ are shown together in Fig. 4. The FDTD simulations clearly show that the electric field is weakly confined in the conelike resonators in sample $S_{S,1}$, and consequently the zone center optical phonon in the Si substrate beneath the resonators would have a major contribution to the overall optical response of sample $S_{S,1}$. Therefore, the

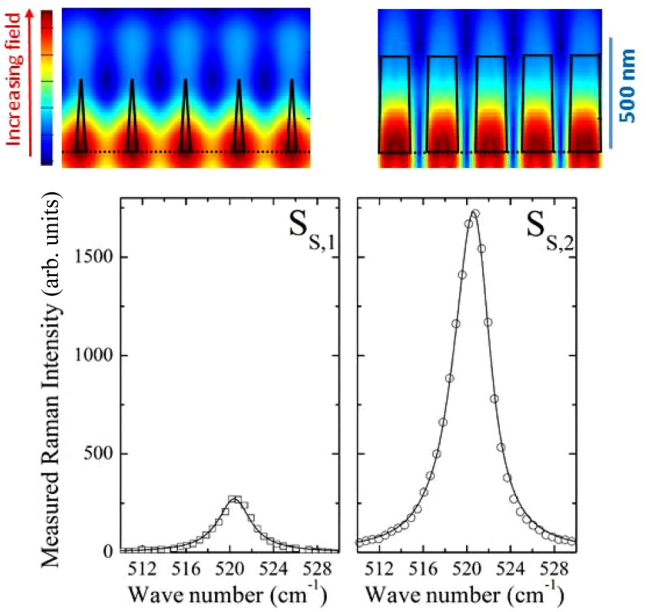

FIG. 4. Finite-difference time-domain (FDTD) simulations of the electric field distribution in the samples of the first set, and the Raman spectra corresponding to the samples of the first set. The dashed lines in the FDTD simulations indicate the interface between the resonators and the Si substrate. The solid lines in the FDTD simulations indicate the resonators' shape. A scale of 500 nm is introduced to visualize the resonators' size. The symbols indicate the measured Raman spectra. The solid lines indicate the calculated Raman spectra using the spatial correlation model.

Raman spectrum taken from sample $S_{S,1}$ does not differ much from that taken from a bare Si substrate. It exhibits neither an appreciable Raman enhancement nor a downshift and broadening. However, a stronger field confinement can be noticed in the pillarlike resonators in sample $S_{S,2}$. Therefore, the corresponding Raman spectrum exhibits Raman enhancement (a signature of field confinement in the resonators) and a downshift and broadening (a signature of phonon confinement in the resonators). Thus, in the first sample set, interaction between confined photons and confined phonons is observed only in pillarlike resonators.

Several models can be used to quantify the size of the crystallites confining phonons in the pillarlike resonators from the downshift and broadening of the Raman spectrum. The most popular ones are the microscopic force model [55], the bond polarization model [56–58], and the spatial correlation models [41,59]. The spatial correlation models, however, have the advantage that they are less affected by some strong assumptions and approximations such as the continuum medium approximation. Therefore, we adopted a spatial correlation model to deduce from the downshift and broadening of the measured Raman spectrum the crystallites' size distribution in the surface layers of the resonators. In the Appendix, we detail the spatial correlation model used in this work. The spatial correlation model was fitted to the measured Raman spectra using the linear least-squares method with adjusting only the parameters that determine the lognormal function describing the crystallites' size distribution (i.e., the most probable size and the skewness of the distribution). The spectra intensities were taken from the measurements. The good agreement between the calculated and measured Raman spectra is demonstrated in Fig. 4. We show in Table I the parameters of the crystallites' size distribution obtained by fitting the spatial correlation model to the measured Raman spectra. The scatter in the experimental data points dominated the uncertainties on the measurements and on the derived crystallites' size distributions. They are estimated to not exceed 3%.

B. Effect of the resonator shape in the second set of samples (resonator heights ranging between 800 and 875 nm)

The Raman spectra and FDTD simulations of the field distribution for the samples of the second set (samples $S_{M,1}$, $S_{M,2}$, and $S_{M,3}$) are shown in Fig. 5. We recall here that the height of the resonators in this set is greater than that of the resonators in the first set (see Table I). The FDTD simulations in Fig. 5 demonstrate that a noticeable amount of the incident electric field is confined in the conelike resonators in sample $S_{M,1}$. Therefore, the corresponding Raman spectrum exhibits a significant Raman enhancement accompanied by a downshift and broadening. The Raman enhancement is due to electric field confined in the conelike resonators, whereas the downshift and broadening of the Raman spectrum is due to light interaction with phonons confined in nanosized crystallites in the conelike resonators. Thus, unlike the conelike resonators of the first set, the conelike resonators of the second set can promote interaction between confined electric field and phonons confined in nanosized crystallites. The FDTD simulations in Fig. 5 also demonstrate that the field confinement gets stronger as the resonators become more pillarlike. The results of the FDTD

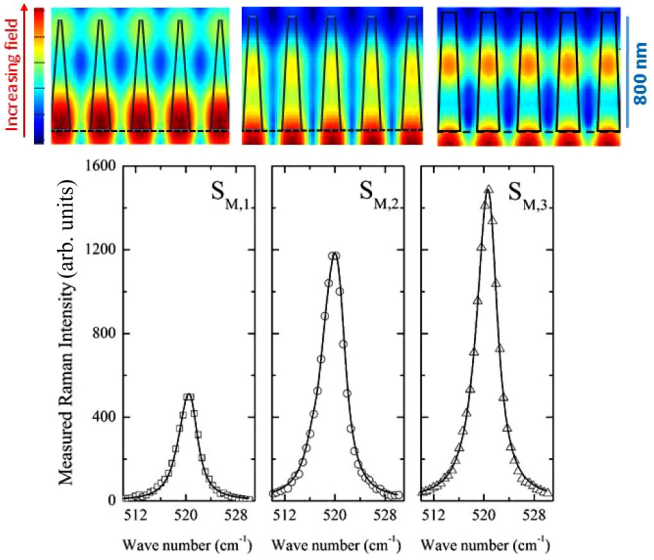

FIG. 5. Finite-difference time-domain (FDTD) simulations of the electric field distribution in the samples of the second set, and the Raman spectra corresponding to the samples of the second set. The dashed lines in the FDTD simulations indicate the interface between the resonators and the Si substrate. The solid lines in the FDTD simulations indicate the resonators' shape. A scale of 800 nm is introduced to visualize the resonators' size. The symbols indicate the measured Raman spectra. The solid lines indicate the calculated Raman spectra using the spatial correlation model.

simulations are supported by the Raman measurements, which demonstrate that the Raman enhancement gets stronger as the diameter of the resonators at the top approaches the diameter of the resonators at the bottom. The spatial correlation model was fitted to the Raman spectra of the samples of the second set using the linear least-squares method with adjusting the parameters determining the lognormal size distribution function. A very satisfactory agreement between the calculated and measured Raman spectra was obtained. The calculated Raman spectra are plotted in Fig. 5 using solid lines. The crystallites' size in each of the measured samples obtained from fitting the spatial correlation model to the measured Raman spectra is indicated in Table I. We found a size distribution only for the sample having pillarlike resonators (sample $S_{M,3}$). The other samples of the second set showed monodisperse crystallites.

C. Effect of the resonator shape in the third set of samples (resonator heights ranging between 1150 and 1280 nm)

The samples in the third set have the highest resonators. The Raman spectra and FDTD simulations of the field distribution for the samples of this set (samples $S_{L,1}$, $S_{L,2}$, and $S_{L,3}$) are shown in Fig. 6. Both Raman spectra and FDTD simulations demonstrate that the resonators of the samples in the third set are remarkably more efficient in electric field confinement than the resonators of the samples of the first and second set. However, similar to the first and second set, the field confinement gets stronger as the resonators become more pillarlike. The measured Raman spectra of the samples of the third set were analyzed using the spatial correlation model, and the crystallites' sizes in the measured samples were

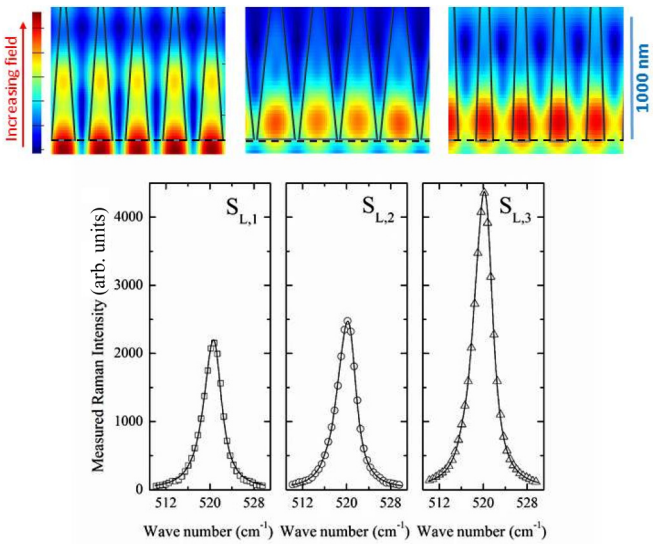

FIG. 6. Finite-difference time-domain (FDTD) simulations of the electric field distribution in the samples of the third set, and the Raman spectra corresponding to the samples of the third set. The dashed lines in the FDTD simulations indicate the interface between the resonators and the Si substrate. The solid lines in the FDTD simulations indicate the resonators' shape. A scale of 1000 nm is introduced to visualize the resonators' size. The symbols indicate the measured Raman spectra. The solid lines indicate the calculated Raman spectra using the spatial correlation model.

obtained by fitting the spatial correlation model to the measured Raman spectra. The calculated Raman spectra are plotted in Fig. 6 using solid lines, and the obtained crystallites' sizes in each of the measured samples are indicated in Table I. We notice that among all the measured samples, sample $S_{L,3}$, which is characterized by the highest pillarlike resonators, best ensures the desirable interaction between confined photons and confined phonons.

D. Comparative evaluation of the effect of resonators' size and shape on the interaction between confined photons and confined phonons

The Raman measurements and FDTD simulations carried out on the samples investigated in this work revealed important information about the effect of the resonators' shape and size on the confinement of photons and phonons. By comparing the FDTD simulations and the Raman enhancements shown in Figs. 4–6, we notice that the field confinement gets stronger as the resonator height is increased. On the other hand, by comparing the FDTD simulations and Raman enhancements shown in each of Figs. 4–6, we notice that the field confinement gets stronger as the resonator shape becomes cylindrical. Moreover, we can notice from Fig. 6 that, although the volume of the resonators of sample $S_{L,2}$ is greater than that of the resonators of sample $S_{L,3}$, the confinement of the electric field in sample $S_{L,2}$ is weaker than that in sample $S_{L,3}$. These results suggest the following. While the volume of the resonators does not present an appreciable effect on the electric field confinement in the resonators, the height and shape of the resonators are key parameters determining the strength of the field confinement in the dielectric resonators. The confinement of the electric field augments as the resonators increase in height and their shape becomes cylindrical. We believe that this is because the highest cylindrical resonators can attain the greatest oscillation amplitude, which is the prime determinant of field confinement. As the resonators' height decreases and their shape deviates from the ideal cylindrical shape, the resonators lose their ability to vibrate, and consequently lose their efficiency in confining the incident electric field.

The resonators in the samples investigated are microsized. They are all too large to confine phonons. Thus, when the effects of laser heating and Fano resonance are ruled out, there will be no reason that any of the investigated resonator arrays induce Raman shift and broadening.

The Raman downshift and broadening are due exclusively to phonon confinement in defective regions located in the surface layer of the Si resonators. Phonon confinement in crystallites of comparable average sizes was observed in all the measured samples. This suggests that the resonators' size and shape do not have an appreciable effect on the spatial correlation length in the resonators. This is due to the fact that the characteristics of the defective regions in the surface layer of the resonators do not depend on the resonators' size and shape. They depend only on the surface structuring technique. However, by comparing the FDTD simulations in Figs. 4–with the corresponding crystallites' size distributions in Table I, we notice that the skewness of the size distribution increases as the confined electric field spreads in the resonators. This can be understood if we realize that the damage in the resonator surface layers induced by the structuring process is not uniform over the resonator height. Hence, when the electric field spreads in the resonators it interacts with phonons confined in crystallites of different sizes.

The Raman downshift and broadening are due exclusively to phonon confinement in defective regions located in the surface layer of the Si resonators. The characteristics of these defective regions, which are induced by the reactive ion etching, do not depend on the resonators' size and shape. They depend only on the surface structuring technique. Therefore, the observed Raman shift and broadening are expected to be independent of the resonators' size and shape. The observed Raman downshift and broadening are due exclusively to phonon confinement in defective regions located in the surface layer of the Si resonators.

As a result, long cylindrical resonators arranged on two-dimensional lattice points over a large area present great potential for confining an important amount of the incident electric field and promoting the interaction between the confined electric field and phonons confined in nanosized crystallites in the surface layers of the resonators. Such an interaction significantly enhances the photovoltaic processes in Si because it strongly amplifies the number of photons interacting with Si and does not require total momentum conservation.

E. Electric field confinement causes substantial crystallite heating in the resonators

It is now well known that high laser powers can accumulate an important amount of energy in nanosized crystallites (because of their low thermal properties), and hence distort their Raman spectrum by strengthening the effects of laser

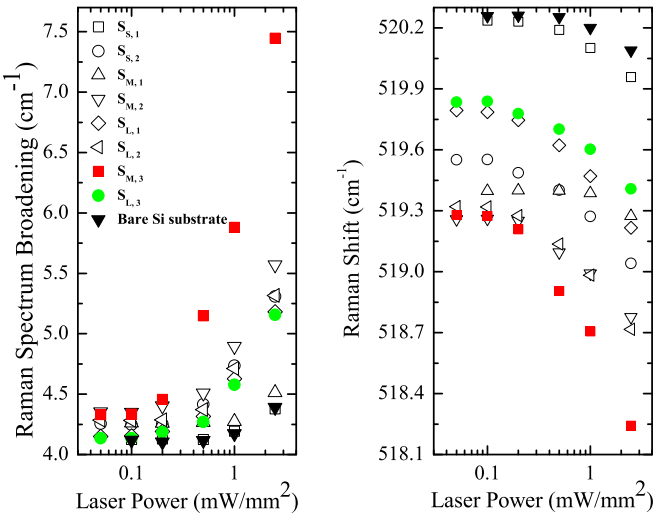

FIG. 7. Raman shift and spectrum broadening versus the incident laser power.

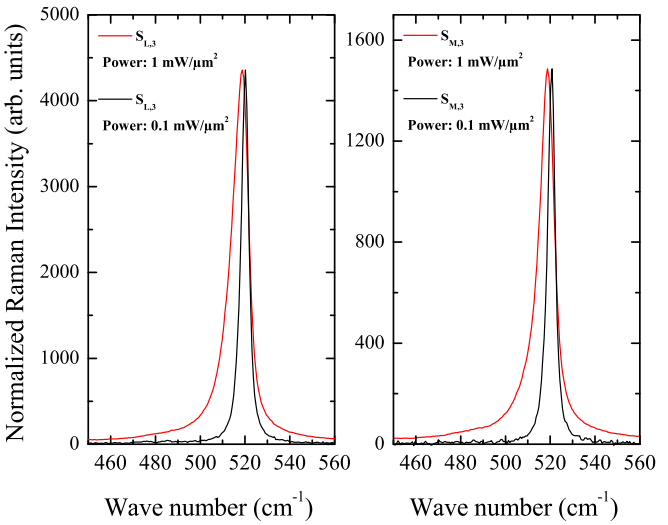

FIG. 8. Raman spectra of samples $S_{M,3}$ and $S_{L,3}$ measured with a laser power of 1 mW/μm^2 and 0.1 mW/μm^2. The spectra are normalized for the sake of comparison.

heating and Fano resonance. It was found that the threshold power for the effects of laser heating and Fano resonance in nanosized Si crystallites is about 1 mW/μm^2 [44,45]. As mentioned previously, in order to rule out the effect of laser heating and laser-induced Fano resonance, we have decreased the excitation laser power successively until the Raman shift and line shape became independent of laser power. In Fig. 7 we plot the measured Raman shift and spectrum broadening versus the incident laser power. As can be noticed, the Raman shift and spectrum broadening become independent of laser power only for laser powers lower than approximately 0.2 mW/μm^2. This implies that the effects of Fano resonance and laser heating on the measured Raman shift and line shape vanish completely only for a laser power lower than 0.2 mW/μm^2, which is five times lower than the reported threshold power for the effects of laser heating and Fano resonance in nanosized Si crystallites. Based on the discussion above, we attribute the existence of effects of Fano resonance and laser heating at such low laser powers to the fact that the electric field confinement in the resonators significantly increases the temperature of the crystallites embedded in the resonators. In Fig. 8, we show the Raman spectra of samples $S_{M,3}$ and $S_{L,3}$ (the samples with pillarlike resonators, which showed the strongest field confinement) measured with a laser power of 1 mW/μm^2 (the reported threshold power for the effects of laser heating and Fano resonance) and a laser power of 0.1 mW/μm^2. The spectra are normalized for the sake of comparison. The spectra measured with a laser power of 1 mW/μm^2 are heavily distorted. A downshift and asymmetric broadening relative to the spectra measured with a laser power of 0.1 mW/μm^2 can be clearly noticed. This further highlights the strength of the electric field that can be confined in arrays of dielectric resonators.

IV. CONCLUSION

Raman spectra from large arrays of dielectric Si resonators attached to Si substrates showed an appreciable Raman enhancement accompanied by a downshift and broadening relative to the Raman spectrum from a bare Si substrate. FDTD simulations demonstrated that the collective lattice resonance induces an efficient field confinement in the resonators, which results in an appreciable Raman enhancement. A spatial correlation model demonstrated that the spectrum downshift and broadening is the result of the relaxation of the phonon wave vector, which is due to phonon confinement in nanosized Si crystallites in the surface layers of the resonators. The effect of the resonators' size and shape on the confinement of photons and phonons was investigated. It was demonstrated that, as the resonators increase in height and their shape becomes cylindrical, the amplitude of their coherent oscillation increases and hence their ability to confine the incoming electric field increases. However, it was found that the resonators' shape and size do not have a remarkable effect on phonon confinement. The results presented in this work show that large arrays of long, cylindrical, dielectric Si resonators drastically suppress the light scattering losses by field confinement and promote the interaction of the confined field with confined phonons. The results highlighted in this paper are expected to help to gain more insight into the confinement of phonons and photons and rationally design metasurfaces for high-efficiency optical devices. For instance, the observed amplified photon-phonon nonconservative interaction mechanism has great potential for strongly enhancing the photovoltaic effect in Si.

ACKNOWLEDGMENTS

We acknowledge financial support by the National Council for Scientific Research (CNRS-Lebanon), The American University of Beirut through a URB grant, The Champagne-Ardenne regional Council and the European Social Fund through the projects SYNAPSE (D201207251) and TEZO (E201211445 and E201211419) and a fellowship to M.T. at UTT. We also would like to thank Nano'mat platform for the RIE equipment and L. Le Cunff for discussion on FDTD simulations.

APPENDIX: SPATIAL CORRELATION MODEL USED IN THE CALCULATION OF THE PHONON CONFINEMENT IN THE SILICON RESONATORS

The wave function of a Raman active phonon mode of wave vector $\mathbf{q}_0$ in an infinite crystal can be written in the form

$$\Phi(\mathbf{q}_0,r) = u(\mathbf{q}_0,r)\exp(-i\mathbf{q}_0 r), \tag{A1}$$

where $u(\mathbf{q}_0,r)$ is the amplitude of the wave function having crystal periodicity. According to the spatial correlation model, it becomes

$$\Psi(\mathbf{q}_0,r) = \Theta(r,D)\Phi(\mathbf{q}_0,r) = \Psi'(\mathbf{q}_0,r)u(\mathbf{q}_0,r), \tag{A2}$$

in a finite crystal of size D, where $\Theta(r,D)$ is the phonon weighting function describing the strength of phonon confinement in the finite crystal (here we assume a finite spherical crystal). The function $\Psi'(\mathbf{q}_0,r)$ in Eq. (2) can be expanded in a Fourier series and written in the form

$$\Psi'(\mathbf{q}_0,r) = \int C(\mathbf{q}_0,\mathbf{q})\exp(i\mathbf{q}r)d^3q, \tag{A3}$$

where the Fourier coefficients $C(\mathbf{q}_0,\mathbf{q})$ are given by

$$C(\mathbf{q}_0,\mathbf{q}) = \frac{1}{(2\pi)^3}\int \Psi'(\mathbf{q}_0,\mathbf{q})\exp(-i\mathbf{q}r)d^3r. \tag{A4}$$

The importance of Eq. (4) stems from the fact that it demonstrates that while the Raman spectrum from an infinite crystal is determined by a phonon wave function, a phonon wave packet formed by a superposition of eigenfunctions with wave vectors $\mathbf{q}$ centered at $\mathbf{q_0}$ determines the Raman spectrum from a finite crystal. In principle, the introduction of the phonon weighting function breaks the translational symmetry and imposes that the integral in Eq. (4) extends from $-\infty$ to $+\infty$. However, if the size of the finite crystal under consideration is at least one order of magnitude greater than the lattice constant, the bulk phonon dispersion can be adopted within the spatial correlation length model, and the integration can be performed over the wave vectors within the Brillouin zone only. Upon using Eqs. (1)–(4), it can be found that if the first-order Raman spectrum from an infinite crystal is given by

$$I_{\text{inf}}(\omega) \propto \frac{1}{\pi}\frac{\frac{1}{2}\Gamma}{[\omega(\mathbf{q}_0)-\omega]^2+\left(\frac{1}{2}\Gamma\right)^2}, \tag{A5}$$

the first-order Raman spectrum from a finite crystal is given by

$$I(\omega) \propto \int |C(\mathbf{q}_0,\mathbf{q})|^2 L(\omega,\mathbf{q})\cdot d^3q, \tag{A6}$$

where Γ is the zone center optical phonon damping, $\omega(\mathbf{q}_0)$ is the zone center optical phonon frequency, and $L(\omega,\mathbf{q})$ is given by

$$L(\omega,\mathbf{q}) = \frac{1}{\pi}.\frac{\frac{1}{2}\Gamma}{[\omega(\mathbf{q})-\omega]^2+\left(\frac{1}{2}\Gamma\right)^2}. \tag{A7}$$

It can be clearly noticed from Eqs. (5) and (6) that the Raman scattering from an infinite material is a process in which the total momentum is conserved (it involves the contribution of only $\mathbf{q}\approx 0$ phonons to keep the total momentum conserved). However, the Raman scattering process from a finite crystal does not require momentum conservation and involves contribution from optical phonons away from the Brillouin zone center. In order to account for a possible distribution of crystal sizes in the resonators, we express the first-order Raman spectrum as

$$I(\omega) \propto \int_0^\infty F(D)\left[\int |C(\mathbf{q}_0,\mathbf{q})|^2 L(\omega,\mathbf{q})\cdot d^3q\right]dD. \tag{A8}$$

It has been demonstrated that a lognormal function best describes the size distribution of Si nanocrystals embedded in a given matrix [60–62]. Therefore, we write the size distribution $F(D)$ in the form of a lognormal function as

$$F(D) = \frac{1}{\sigma}\exp\left(-\left[\frac{(\log D-\log\bar{D})^2}{2\sigma^2}\right]\right), \tag{A9}$$

where $\bar{D}$ is the most probable size and σ is the skewness of the size distribution.

Several attempts have been made to establish a universal form for the phonon weighting function $\Theta(r,D)$. The most physically accepted forms are that of Faraci *et al.* [63–65] and that of Roodenko *et al.* [66]. In our calculation, we adopt the form of the phonon weighting function established by Roodenko *et al.* because it has the advantage of easier numerical implementation. In order to express $\omega(\mathbf{q})$ with taking into account the anisotropy of the phonon dispersion in silicon, we use the method of Paillard *et al.* [67], which is based on the Brout sum rule to accurately average over different phonon branches in high-symmetry crystallographic directions [68].

[1] A. K. Arora, M. Rajalakshmi, T. R. Ravindran, and V. Sivasubramanian, J. Raman Spectrosc. **38**, 604 (2007).
[2] E. Yablonovitch, J. Opt. Soc. Am. **72**, 899 (1982).
[3] W. H. Southwell, J. Opt. Soc. Am. A **8**, 549 (1991).
[4] P. B. Clapham and M. C. Hultey, Nature **244**, 281 (1973).
[5] A. R. Parker and H. E. Townley, Nat. Nanotechnol. **2**, 347 (2007).
[6] Y.-F. Huang, S. Chattopadhyay, Y.-J. Jen, C.-Y. Peng, T.-A. Liu, Y.-K. Hsu, C.-L. Pan, H.- C. Lo, C.-H. Hsu, Y.-H. Chang, C.-S. Lee, K.-H. Chen, and L.-C. Chen, Nat. Nanotechnol. **2**, 770 (2007).
[7] J.-Q. Xi, M. F. Schubert, J. K. Kim, E. F. Schubert, M. Chen, S.-Y. Lin, W. Liu, and J. A. Smart, Nat. Photonics **1**, 176 (2007).
[8] T.-H. Her, R. J. Finlay, C. Wu, S. Deliwala, and E. Mazur, Appl. Phys. Lett. **73**, 1673 (1998).
[9] H. M. Branz, V. E. Yost, S. Ward, K. M. Jones, B. To, and P. Stradins, Appl. Phys. Lett. **94**, 231121 (2009).
[10] H.-C. Yuan, V. E. Yost, M. R. Page, P. Stradins, D. L. Meier, and H. M. Branz, Appl. Phys. Lett. **95**, 123501 (2009).
[11] S. Koynov, M. S. Brandt, and M. Stutzmann, Appl. Phys. Lett. **88**, 203107 (2006).

[12] R. Shuker and R. W. Gammon, Phys. Rev. Lett. **25**, 222 (1970).
[13] K. K. Tiong, P. M. Amirtharaj, F. H. Pollak, and D. E. Aspnes, Appl. Phys. Lett. **44**, 122 (1984).
[14] H. A. Atwater and A. Polman, Nat. Mater. **9**, 205 (2010).
[15] K. T. Carron, W. Fluhr, M. Meier, A. Wokaun, and H. W. Lehmann, J. Opt. Soc. Am. B **3**, 430 (1986).
[16] S. L. Zou, N. Janel, and G. C. Schatz, J. Chem. Phys. **120**, 10871 (2004).
[17] S. L. Zou and G. C. Schatz, Chem. Phys. Lett. **403**, 62 (2005).
[18] P. Spinelli, M. A. Verschuuren, and A. Polman, Nat. Commun. **3**, 692 (2012).
[19] F. J. Bezares, J. P. Long, O. J. Glembocki, J. Guo, R. W. Rendell, R. Kasica, L. Shirey, J. C. Owrutsky, and J. D. Caldwell, Opt. Express **21**, 27587 (2013).
[20] A. I. Kuznetsov, A. E. Miroshnichenko, M. L. Brongersma, Y. S. Kivshar, and B. Luk'yanchuk, Science **354**, 846 (2017).
[21] A. B. Evlyukhin, C. Reinhardt, A. Seidel, B. S. Luk'yxanchuk, and B. N. Chichkov, Phys. Rev. B **82**, 045404 (2010).
[22] S. Tsoi, F. J. Bezares, A. Giles, J. P. Long, O. J. Glembocki, J. D. Caldwell, and J. Owrutsky, Appl. Phys. Lett. **108**, 111101 (2016).
[23] S. G. Cloutier, C.-H. Hsu, P. A. Kossyrev, and J. Xu, Adv. Mater. **18**, 841 (2006).
[24] S. G. Cloutier, R. S. Guico, and J. M. Xu, Appl. Phys. Lett. **87**, 222104 (2005).
[25] M. Hofmann, Y.-P. Hsieh, C.-T. Liang, and Y.-F. Chen, J. Raman Spectrosc. **44**, 81 (2013).
[26] D. Banerjee, C. Trudeau, L. F. Gerlein, and S. G. Cloutier, Appl. Phys. Lett. **108**, 113109 (2016).
[27] A. L. Bassi, D. Cattaneo, V. Russo, C. E. Bottani, E. Barborini, T. Mazza, P. Piseri, P. Milani, F. O. Ernst, K. Wegner, and S. E. Pratsinis, J. Appl. Phys. **98**, 074305 (2005).
[28] M. J. Šćepanović, M. G. Brojčin, Z. D. Dohčević-Mitrović, and Z. V. Popović, Appl. Phys. A **86**, 365 (2007).
[29] A. C. A. Silva, E. S. F. Neto, S. W. da Silva, P. C. Morais, and N. O. Dantas, J. Phys. Chem. C **117**, 1904 (2013).
[30] A. Gwiazda, A. Rumyantseva, A. Gokarna, K. Nomenyo, C. Chevalier-César, and G. Lérondel, Adv. Mater. Technol. **2**, 1700107 (2017).
[31] P. G. Klemens, Physica B (Amsterdam, Neth.) **316-317**, 413 (2002).
[32] J. M. Zhang, M. Giehler, A. Göbel, T. Ruf, M. Cardona, E. E. Haller, and K. Itoh, Phys. Rev. B **57**, 1348 (1998).
[33] A. Wellner, V. Paillard, C. Bonafos, H. Coffin, A. Claverie, B. Schmidt, and K. H. Heinig, J. Appl. Phys. **94**, 5639 (2003).
[34] V. Paillard, P. Puech, R. Sirvin, S. Hamma, and P. Roca i Cabarrocas, J. Appl. Phys. **90**, 3276 (2001).
[35] A. Compaan, M. C. Lee, and G. J. Trott, Phys. Rev. B **32**, 6731 (1985).
[36] V. Magidson and R. Beserman, Phys. Rev. B **66**, 195206 (2002).
[37] N. H. Nickel, P. Lengsfeld, and I. Sieber, Phys. Rev. B **61**, 15558 (2000).
[38] M. Kazan, C. Zgheib, E. Moussaed, and P. Masri, Diamond Relat. Mater. **15**, 1169 (2006).
[39] K. Nagata, M. Takei, A. Ogura, and K. Uchida, Jpn. J. Appl. Phys. **53**, 032401 (2014).
[40] H. Richter, Z. P. Wang, and L. Ley, Solid State Commun. **39**, 625 (1981).
[41] I. H. Campbell and P. M. Fauchet, Solid State Commun. **58**, 739 (1986).
[42] P. M. Fauchet and I. H. Campbell, Crit. Rev. Solid State Mater. Sci. **14**, s79 (2006).
[43] S. Piscanec, M. Cantoro, A. C. Ferrari, J. A. Zapien, Y. Lifshitz, S. T. Lee, S. Hofmann, and J. Robertson, Phys. Rev. B **68**, 241312 (2003).
[44] G. Faraci, S. Gibilisco, and A. R. Pennisi, Phys. Rev. B **80**, 193410 (2009).
[45] R. Gupta, Q. Xiong, C. K. Adu, U. J. Kim, and P. C. Eklund, Nano Lett. **3**, 627 (2003).
[46] A. Iskandar, A. Gwiazda, Y. Huang, M. Kazan, A. Bruyant, M. Tabbal, and G. Lerondel, J. Appl. Phys. **120**, 095106 (2016).
[47] S. Hayashi, M. Ito, and H. Kanamori, Solid State Commun. **44**, 75 (1982).
[48] T. Okada, T. Iwaki, T. Yamamoto, H. Kasahara, and K. Abe, Solid State Commun. **49**, 809 (1984).
[49] S. Hayashi and H. Kanamori, Phys. Rev. B **26**, 7079 (1982).
[50] T. Kanata, H. Murai, and K. Kubota, J. Appl. Phys. **61**, 969 (1987).
[51] S. Hayashi and R. Ruppin, J. Phys. C **18**, 2583 (1985).
[52] S. Hayashi, Solid State Commun. **56**, 375 (1985).
[53] S. Hayashi, Jpn. J. Appl. Phys. **23**, 665 (1984).
[54] S. Hayashi and Y. Yamamoto, Superlattices Microstruct. **2**, 581 (1986).
[55] W. Cheng and S.-F. Ren, Phys. Rev. B **65**, 205305 (2002).
[56] J. Zi, K. Zhang, and X. Xie, Phys. Rev. B **55**, 9263 (1997).
[57] J. Zi, H. Büscher, C. Falter, W. Ludwig, K. Zhang, and X. Xie, Appl. Phys. Lett. **69**, 200 (1996).
[58] T. Thonhauser and G. D. Mahan, Phys. Rev. B **71**, 081307 (2005).
[59] P. Parayanthal and F. H. Pollak, Phys. Rev. Lett. **52**, 1822 (1984).
[60] K. W. Adu, H. R. Gutiérrez, U. J. Kim, G. U. Sumanasekera, and P. C. Eklund, Nano Lett. **5**, 409 (2005).
[61] I. Doğan and M. C. M. van de Sanden, J. Appl. Phys. **114**, 134310 (2013).
[62] P. Zhang, Y. Feng, R. Anthony, U. Kortshagen, G. Conibeer, and S. Huang, J. Raman Spectrosc. **46**, 1110 (2015).
[63] G. Faraci, S. Gibilisco, P. Russo, A. R. Pennisi, and S. La Rosa, Phys. Rev. B **73**, 033307 (2006).
[64] G. Faraci, S. Gibilisco, A. R. Pennisi, and C. Faraci, J. Appl. Phys. **109**, 074311 (2011).
[65] G. Faraci, G. Mannino, A. R. Pennisi, R. Ruggeri, P. Sberna, and V. Privitera, J. Appl. Phys. **113**, 063518 (2013).
[66] K. Roodenko, I. A. Goldthorpe, P. C. McIntyre, and Y. J. Chabal, Phys. Rev. B **82**, 115210 (2010).
[67] V. Paillard, P. Puech, M. A. Laguna, and R. Carles. J. Appl. Phys. **86**, 1921 (1999).
[68] R. Brout, Phys. Rev. **113**, 43 (1959).